LES Modelling of Spark-Ignition Cycle-to-Cycle Variability on a Highly Downsized DISI Engine

Author, co-author (Do NOT enter this information. It will be pulled from participant tab in MyTechZone)

Affiliation (Do NOT enter this information. It will be pulled from participant tab in MyTechZone)

Abstract

The paper reports an activity aiming at characterizing cycle-to-cycle variability (CCV) of the spark-ignition (SI) process in a high performance engine. The numerical simulation of spark-ignition and of early flame kernel evolution are major challenges, mainly due to the time scales of the spark discharge process and to the reduced spatial scales of flame kernel. Typical mesh resolutions are insufficient to resolve the process and a dedicated treatment has to be provided at a subgrid level if the ignition process is to be properly modelled. The focus of this work is on the recent ISSIM-LES (Imposed Stretch Spark-Ignition Model) ignition model, which is based on an extension of the flame surface density (FSD) transport equation for a dedicated flame kernel treatment at subgrid scales. The FSD equation is solved immediately after spark discharge. The interaction of the flame kernel with the flow field is fully accounted for since spark formation and a transition is provided from ignition to propagation phase. The comparison is carried out with the AKTIM-Euler ignition model in terms of flame interaction with the flow field (e.g. arc convection, flame blow-off, flame holder effect). A multiple cycle LES activity provided a set of cycle-resolved conditions for spark-ignition comparisons, and the flame kernel development is carefully analyzed for the two ignition models on a wide range of thermo-physical conditions. Spark-ignition cyclic variability and combustion traces are compared with experiments. Results confirm that the simulated cycle-to-cycle variability increases through the adoption of the ISSIM-LES ignition model.

Introduction

The recent legislation (Euro V, Euro VI and forthcoming) is pushing the engine manufacturers towards renewed design concepts for SI engines. These are driven by the downsizing principle, consisting in more compact yet more efficient engines, in order to preserve the original performance target of old generation units with reduced fuel consumption and pollutant emissions. New generation spark-ignition engines achieve these targets by increasing the volumetric compression ratio, by adopting turbocharging systems and by carefully targeting fuel injection to achieve optimized charge stratification. Limitations to these strategies are due to the poor tolerance of SI engines to these approaches because the first two are responsible for the long-known issue of abnormal combustion onset, also called engine knock, while the third is limited by cyclic variability. Knock is essentially due to the self-ignition of pockets of unburnt mixture in the end-gas region of the combustion chamber before the main propagating flame front consumes it. The sudden heat release and the shock pressure waves that are originated are responsible for serious engine failure: metal erosion [1], lubricant film removal and increased thermo-mechanical loading [2, 3] are just the most relevant damaging mechanisms that are caused by gasoline autoignition. The quest for knock-free higher thermal efficiency is made even harder by the non-repeatability of the highly turbulent combustion in SI engines, which is known as cycle-to-cycle variability (CCV). Extended literature surveys on its main causes are given by Young [4] and by Ozdor et al. [5]. The main factors causing combustion CCV can be resumed by the random fluctuation of local physical conditions (i.e. flow field, mixture composition and residual concentration) in the spark plug region during early flame kernel formation. Outlier cycles from the theoretical mean one can give rise to both misfiring events (in the low-end portion of the range induced by CCV) or to abnormal combustion/knock (in the high-end part of the same).

As for the knock-free concern, which is the main interest of high-performance engine such as the one analyzed in this paper, this is avoided by reducing the engine spark time with respect to its theoretical optimal condition, in order to keep a safety margin for faster than average cycles. Nevertheless, a small fraction of knocking cycles is tolerated in order not to dramatically limit the engine performance. This threshold is typically based on the manufacturer experience. The same applies to misfiring cycles, for which tolerances are even narrower due to their dramatic impact on engine-out emissions.

This overview highlights the importance of numerical models able to correctly simulate combustion stability in the earliest portion of flame development. Despite attempts to account for flow variability statistics in a RANS framework, such as the work by Linse et al. [6] regarding knock probability or the Hasse et al. [7] methodology regarding hybrid RANS/LES turbulence modelling, it is believed that the numerical approach for this kind of simulation must necessarily be some sort of Large-Eddy Simulation (LES). A first support to this argument lies in the intrinsic simulation of the spark-ignition process (i.e. flame interaction with the surrounding flow field) that is carried out by LES, instead of some sort of bulk statistics that is transported with the mean flow. In this way cycle-specific events such as misfire of abnormally fast flame formation can be properly simulated. A second reason comes from the maturity of LES models for both subgrid-scale turbulence closure and for flame propagation, which can exploit the relatively low-cost computational power to give unprecedented insight into the underlying physics of the phenomenon

and to suggest new solutions. Extended reviews of the state of art of LES modelling of combustion are given by Rutland [8] and Haworth [9].

The simulation of the spark-ignition process poses several difficulties from a numerical point of view. This is motivated by the extremely short length and time scales of the electric arc and of the initial ionized gas in the surrounding of the spark plug electrodes, as well as their life time, which would make the simulation of these phenomena unaffordable for the commonly adopted grids and time steps. In the illustration of the electric discharge process, Maly [10] points out that the breakdown phase is characterized by time scales in the order of ns and the ionized channel that is formed can reach temperatures up to 60000 K. Therefore, simplifications are usually undertaken in order to represent the spark-ignition phenomenon on commonly adopted CFD codes.

An example of ignition model where the small-scale flame kernel evolution is modelled is the DPIK (Discrete Particle Ignition Kernel) ignition model from Fan et al. [11] and then detailed by Tan and Reitz [12], which is based on a phenomenological transport of discrete Lagrangian particles in order to track the flame kernels evolution. However, the use of discrete kernel trackers is not coherent with the Eulerian concept of flame surface density and the FSD initialization is critical.

A significant modelling complexity is proposed in the SparkCIMM (Spark Channel Ignition Monitoring Model) ignition model by Dahms and co-workers in a series of papers [13, 14, 15]. This includes the creation of multiple local flame kernels along the spark channel and a Lagrangian sub-model accounts for kernels merging in a single larger non-spherical flame front. However, application of this detailed model and not known in the LES context.

From a modelling point of view, the simplest approach to model spark-ignition is to instantaneously impose a small fully burnt volume in order to initialize the combustion model. Examples of such models are the Local Energy Deposit Ignition (LEDI) adopted by Thobois et al. [16] and later by Goryntsev et al. [17] and the AKTIM-Euler ignition model [18, 19], which is illustrated in more detail in the Numerical Setup section and which will be adopted for a part of the presented simulations. An unavoidable drawback of this family of ignition models is in the finite dimension of the initially imposed burnt volume, which must be of the order of the cell size in the spark plug region in order to be filtered and correctly resolved on the grid. This implies the complete lack of the modelling of the phase preceding the flame kernel growth up to that size. This in turn affects not only on the combustion phasing (a portion of flame life time is not simulated at all) but also the combustion CCV of the early flame kernel: the rigid imposition of a burnt gas profile smears out all the potential deviations in flame evolution up to that point.

An alternative strategy identified by the authors in [20] was to counterbalance the use of the AKTIM-Euler model by adopting a strong mesh refinement (as low as 0.08 mm) in the spark plug region. This strategy effectively limited the size of the filtered flame kernel and the FSD equation handled its propagation since the first stage. Despite the CPU cost due to the grid refinement, a significant improvement of CCV was measured with this technique when compared to experimental measurements.

A relevant attempt to overcome the difficulties of the flame deposition models is the recent ISSIM-LES (Imposed Stretch Spark-Ignition Model) [21] ignition model for early flame kernel propagation. It consists of the use of a modified FSD equation, accounting both for early flame evolution, at subgrid scales for typical engine grids, and for flame propagation, where the standard FSD equation is recovered. Further details of the model will be given in the next section. From a general perspective, a wider set of flame kernel-related phenomena are expected from a simulation with ISSIM-LES ignition model. Given the relevance of flame variability that is originated in the initial combustion stages, it is believed that the adoption of models such as ISSIM-LES could represent a relevant improvement in the simulation of combustion irregularity.

The paper is organized as follows. In the next section the details of the presented numerical simulations are outlined, with emphasis on the fundamentals of AKTIM-Euler and ISSIM-LES ignition models. Later, a first validation of the ISSIM-LES model is carried out against experiments in a homogeneous isotropic turbulent field. Finally, engine cases are presented for a currently produced GDI unit, for which experimental data are available at knock-limited spark-advance and combustion CCV is clearly visible. Statistics on combustion instability are made possible by the large number of consecutive cycles acquired by the experimental campaign. Preliminary results from a Large-Eddy Simulation dataset with ISSIM-LES ignition model are presented and compared to the experiments, both in terms of average combustion development and its CCV. Finally, a comparison between ISSIM-LES and AKTIM-Euler ignition models is carried out regarding flame development and the degree of combustion variability. The analysis is focused on the two most different spark-ignition realizations that are available and the simulation improvement allowed by ISSIM-LES is highlighted.

Numerical Setup

The numerical analyses presented in this study are carried out by means of a customized version of the commercial CFD code Star-CD v4.20, licensed by CD-adapco. The computational domain for Large-Eddy Simulation on the engine case is composed by approx. 1M cells at TDC and 1.5M at BDC. The numerical grid adopted considers both the intake and the exhaust ports. As for the last, the full geometry up to the turbine inlet section is modelled, since experimental pressure acquisition was measured in this location. The average cell size is about 0.55 mm both in the cylinder and in the ports regions. No symmetry planes are introduced due both to the inherent randomness of flow realizations when adopting Large-Eddy Simulation and to the asymmetry of the exhaust port configuration. Mesh motion is handled by an Arbitrary Lagrangian-Eulerian (ALE) approach by the *es-ice* plug-in. The adopted time-step is approx. 1e-6 s, although this is further reduced in the proximity of valve opening or closure events. The complete mesh and a close-up on the cylinder domain are represented in Figure 1. Subgrid-scale turbulence is modelled by the algebraic Smagorinsky model [22], with C_s constant equal to 0.202. Despite the limitations inherent with the model simplicity, above all the excessive subgrid energy dissipation and the lack of a subgrid kinetic energy budget, its stability still constitutes a valuable point for such CPU-intensive analyses. The combustion model adopted for all the presented simulations is ECFM-LES [18, 19], which maintains the flame surface density (FSD) formalism of the ECFM-family combustion models widely adopted in RANS analyses with dedicated subgrid-scale terms for transport, stretch and curvature. A set of hybrid boundary conditions for pressure and temperature is adopted: pressure is experimentally measured by mean of fast-response pressure transducers located in the intake/exhaust ports, while for temperature a 1-D time-varying profile is derived from a tuned model in use by the engine manufacturer.

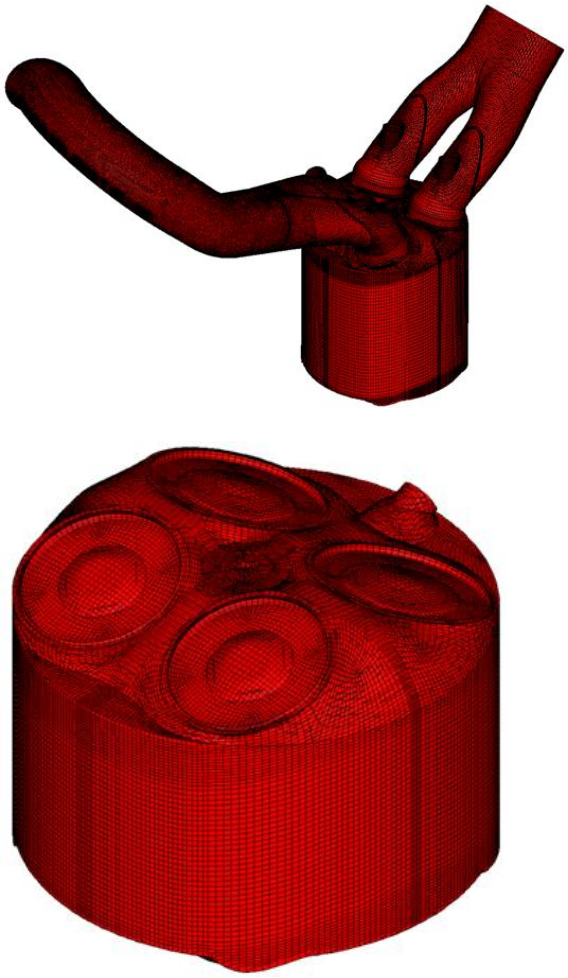

Figure 1. Numerical grid used for LES simulations. Top: complete domain; bottom: close-up on the cylinder domain.

Uniform wall temperatures are imposed for each metal component, while wall heat transfer is modelled through the Angelberger et al. [23] approach. Two-phase flow is accounted for by a pre-atomized population of droplets imposed at each nozzle exit, whose validation is reported in [24], while the Reitz and Diwakar model [25] is used for secondary break-up. It is important to underline that the simulation of fuel injection is performed without any external imposed perturbation, i.e. the mixture stratification and the resulting degree of CCV are the result of the interaction with the turbulent cycle-dependent flow field. Second-order TVD-based numerical schemes are used for momentum discretization, while density is calculated with a central differencing scheme; first order time-integration is adopted. The CPU time for a single full-cycle simulation requires approx. 36 hours on a 48-core Linux cluster.

Finally, the validity of the adopted numerical framework is verified by means of the Energy Resolution (ER) criterion as proposed by Pope [26]. The ensemble average results from the calculated dataset at approx. 600 CA and 670 CA during the compression stroke are reported in Figure 2.

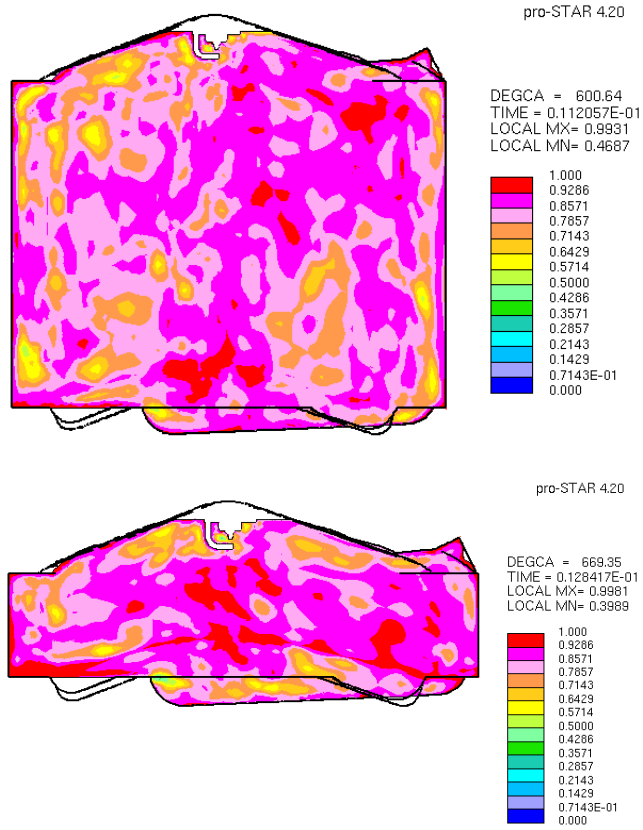

Figure 2. Energy Resolution (ER) field on an axial section for different CA positions. Top: 600 CA; bottom: 670 CA.

A fraction of approx. 80% of the flow turbulent kinetic energy is simulated by the filtered momentum equation, instead of being modelled by the subgrid-scale closure model. This is in line with the recommendations by Pope. Therefore, the present grid is judged as adequate for the modelling of the presented flow realizations. Finally, it is worthwhile to mention that several other mesh quality validation indices in the context of LES are proposed in literature in addition to the widespread ER criterion, and a detailed survey of these can be found in [27].

ISSIM-LES Ignition Model

The ISSIM-LES ignition model was first proposed by Colin and Truffin [21], who exploited the theoretical ability of the FSD equation to model flame propagation since the early stages. A modified FSD transport equation was proposed (Eq. 1) for the temporal variation of the filtered FSD $\bar{\Sigma}_{\tilde{c}}$. This is able to handle both the ignition phase, during which the volume burnt by the spark energy is excessively small to be resolved on common engine grids and for which a dedicated subgrid-scale treatment is proposed, and the resolved flame front during propagation.

$$\frac{\partial \bar{\Sigma}_{\tilde{c}}}{\partial t} = T_{res} + T_{sgs} + S_{sgs} + \alpha C_{sgs} - \nabla \cdot (\alpha S_d N \bar{\Sigma}_{\tilde{c}}) + \alpha (C_{res} + S_{res}) + (1-\alpha)\frac{2}{r_b}(1+\tau)\Xi s_L \bar{\Sigma}_{\tilde{c}} + \dot{\omega}_{\Sigma}^{ign} \quad (1)$$

In Eq. 1 T_{res}, T_{sgs}, C_{res}, C_{sgs}, S_{res}, S_{sgs} are terms related to the standard FSD transport equation for LES proposed in [18, 19]. They account for resolved and subgrid FSD transport (T_{res} and T_{sgs}), curvature (C_{res}

and C_{sgs}) and stretch (S_{res} and S_{sgs}), respectively. As stated earlier, the focus of this work is on the ISSIM-LES model implementation, which requires the addition of new contributions and/or the modification of existing terms.

An additional term $\frac{2}{r_b}(1+\tau)\Xi s_L$ is introduced with respect to the standard FSD equation proposed in [18, 19]. It considers the subgrid curvature contribution to FSD creation given by $2/r_b$, the expansion ratio $\tau = \rho_u/\rho_b - 1$, the turbulent wrinkling factor Ξ and the laminar flame speed s_L. In particular, the wrinkling factor is imposed equal to 1 for this preliminary implementation: this implies that the FSD production due to subgrid turbulence is underestimated and it is the object of current analyses aiming at model improvement. The laminar flame speed s_L is calculated following the relationship proposed by Metghalchi and Keck [28] for isooctane. Finally, the source term $\dot{\omega}_\Sigma^{ign}$ accounts for the FSD creation at spark time following a spherical shape assumption for the flame kernel as proposed in [21]. This expression guarantees a correct representation of the subgrid-scale FSD generation during the ignition when the flame can be approximated by an expanding sphere modelled at subgrid level.

The transition between the subgrid-scale and the resolved level is governed by a continuous ad-hoc α-function, varying from 0 to 1 for ignition and propagation phase, respectively. The α-function is dependent on the equivalent flame radius r_b, which is calculated assuming a spherical shape for the flame following Eq. 2:

$$r_b = \sqrt[3]{\frac{3}{4\pi}\cdot V_{flame}} \tag{2}$$

During spark discharge, the initial kernel radius $r_{b,ign}$ is initialized following the same spherical kernel assumption and it is derived from an initial distribution of filtered progress variable $\tilde{c}_{ign}$ respecting the condition in Eq. 3.

$$\frac{4}{3}\pi r_{b,ign}^3 = \int \tilde{c}_{ign}\, dV \tag{3}$$

The α-function is deputed to the suppression of erroneous terms during the subgrid/ignition phase while activating a dedicated FSD term for subgrid stretch during ignition. As the flame radius increases, a smooth transition is carried out to recover the standard FSD equation. The same α-function definition as the one proposed in [21] is adopted in this study. It follows Eq. 4 and it is represented in Figure 3.

$$\alpha(r_b^+) = 0.5\cdot\left[1 + tanh\left(\frac{r_b^+ - 0.75}{0.15}\right)\right] \tag{4}$$

$$r_b^+ = r_b/\widehat{\Delta} \tag{5}$$

In Eq. 5 r_b^+ is the flame radius resolved at the combustion filter size $\widehat{\Delta}$, which is typically higher than the cell size Δ. In this study $\widehat{\Delta} = 5\cdot\Delta$. However, it is important to underline that this function is not based on physical arguments, its only requirements being:

1. $\lim_{r_b^+\to 0}\alpha(r_b^+) = 0$;
2. $\lim_{r_b^+\to +\infty}\alpha(r_b^+) = 1$;
3. Continuous and derivable algebraic function;
4. Asymptote to unity for $r_b^+ \approx 1$.

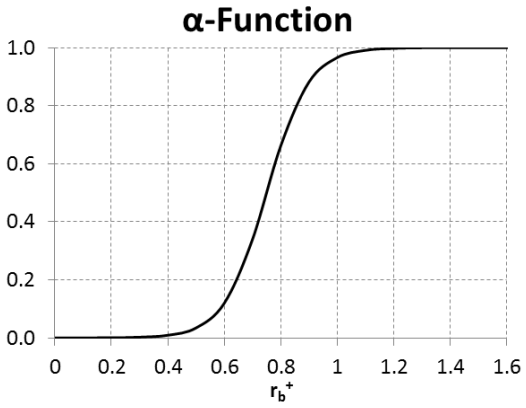

Figure 3. α-function as a function of r_b^+.

Since this function is deputed to switch between subgrid and resolved scales, it should be somehow linked to the filter length, i.e. the local cell size in the flame kernel region. A dynamic version of the α-function, being able to locally adjust the modelling transition based on the filter length, would be an interesting step forward and it is currently under development. The proposed ISSIM-LES model is implemented in Star-CD in a joint cooperation between University of Modena and CD-adapco.

AKTIM-Euler Ignition Model

The AKTIM-Euler (Arc and Kernel Tracking Ignition Model) ignition model is investigated as representative of several spark-ignition models based on the concept of a flame deposition over the resolved flow field in the spark plug region. It was adopted in several publications by the authors on the same engine and operating point as that of this study [20, 29, 30, 31]. The model fundamentals are here briefly resumed for the sake of completeness.

Spark-ignition in AKTIM-Euler is simulated by imposing a profile of fully burnt mixture in the surroundings of the ignition location. The filtered progress variable distribution $\tilde{c}(\bar{x})$ is given by Eq. 6:

$$\tilde{c}(\bar{x}) = \frac{c_0}{2}\left(1 - tanh\frac{\|\bar{x}-\bar{x}_{spk}\|}{r_k}\right) \tag{6}$$

In Eq. 6 the c_0 constant is set to 4 in this work, and it comes from a preliminary conducted sensitivity analysis to this parameter which is not reported for the sake of brevity. The initial flame kernel radius r_k is expressed in Eq. 7 as a function of the laminar flame thickness δ_l and of the ratio between burnt and unburnt temperature (T_b and T_u, respectively).

$$r_k = 15\cdot\delta_l\cdot\frac{T_b}{T_u} \tag{7}$$

This relatively simple ignition model assumes that a successful ignition events is always verified and it lacks in the simulation of the flame kernel development since the initial phase. For typical mesh sizes of approx. 0.5 mm, an early filtered progress variable $\tilde{c}$ much lower than 1 is to be accounted for before a fully burnt flame volume ($\tilde{c}$=1) is present. Conversely, the hypotheses of the AKTIM-Euler

model are the existence of a fully burnt gas profile since spark timing and its rigid imposition on the existing flow field at spark.

In the framework of the simulation of the engine combustion stability resulting from this model, a relatively stiff ignition process is observed. This is due to a self-similar flame development rigidly developing from an invariantly successful kernel deposition event. The reduced combustion CCV measured by the authors in the references studies was attributed to this aspect and in this paper it is critically discussed.

RESULTS

Combustion Bomb Cases

An initial validation of the ISSIM-LES ignition model is carried out against experimental measurements conducted at the Leeds University by Lawes et al [32]. An extended description of their apparatus, the Leeds Mk2 bomb, is reported in Gillespie et al. [33] and Bradley et al. [34]. The fundamental features are here recalled for the sake of completeness. The apparatus is a stainless spherical vessel of inner diameter 380 mm, in which a premixed fuel-air mixture is ignited by means of two centrally mounted electrodes. Three orthogonal pairs of quartz windows are present and they allow optical access for imaging and flame diagnosis. The ignition and flame propagation of several fuels is examined, such as isooctane, methanol and methane. The experiments relevant to the presented validation are carried out at an initial temperature of 360 K and an absolute pressure of 50 bar. An homogeneous isotropic turbulent flow field is produced within the vessel by four fans driven by electric motor. Measurements indicate a velocity fluctuation u' equal to 2 m/s. A premixed isooctane mixture is considered for the current validation, since the similarity of such fuel with those of commercial gasoline (both in terms of physical properties and burning characteristics), while retaining the simplicity of a single-component fuel.

A three-dimensional structured grid is created with hexahedral volumes with uniform cell size of 0.5 mm. The size of the cubic domain is approx. 180x180x180 mm, with a total of about 7M fluid cells. Ignition is triggered in the centroid of the domain, so that a fully three-dimensional and random flame front is allowed for the LES combustion model. In order to reproduce the turbulent environment of the experiments, a statistically homogeneous isotropic turbulent flow field is imposed as initial condition, with a turbulent intensity u' equal to 2 m/s as in the experiments at the University of Leeds. As for the subsequent engine cases, the static Smagorinsky model is adopted for subgrid turbulence with C_s constant equal to 0.202.

The presented simulations are relative to the first phase of flame development. This is firstly motivated by the interest in the earliest portion of flame kernel growth in a turbulent environment. Secondly, this greatly simplifies the numerical simulations: since the flame is not interacting with the domain walls in the early stages, a smaller domain can be simulated and a cubic and perfectly structured grid can be adopted. Moreover, a constant pressure environment is imposed in the simulations in agreement with the experimental observation that a negligible pressure increase is originated in the first portion of the experiment. Finally, a premixed isooctane mixture is evaluated in numerical simulations, for which experiments reported in [32] show a constant pressure period of approx. 5 ms. The equivalent flame radius r_b is calculated as in Eq. 2 and it is reported in Figure 4 as a function of time in the earliest phases of flame life time. The agreement with the experiments is satisfying for the present condition, although an excessively higher flame radius is predicted by the simulation between approx. 0.5 ms and 2.5 ms. This is attributed to the presence of the electrodes in the experimental testing, which are not modelled in the presented simulations. As stated by Gillespie et al. [33] and Bradley et al. [35], flame radius measurement is affected by the electrode presence up to 10 mm. After the initial phase of combustion development, a pressure increase is measured by the experiments in the closed vessel, due to the increasing amount of burnt mixture, and the constant pressure hypothesis of the simulation is no longer valid. For this reason the validation is limited to the initial portion of the experiments. The same simulation is repeated with AKTIM-Euler ignition model, and the flame radius growth in time is reported in Figure 4 for this case as well.

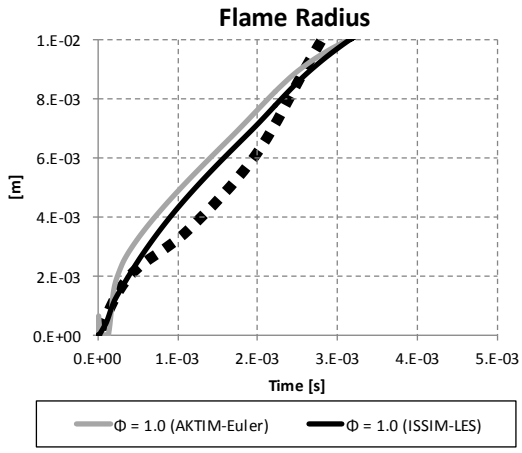

Figure 4. Equivalent flame radius r_b for a stoichiometric isooctane mixture for ISSIM-LES and AKTIM-Euler ignition models. Experiments from [32] are reported for the same mixture (dashed line).

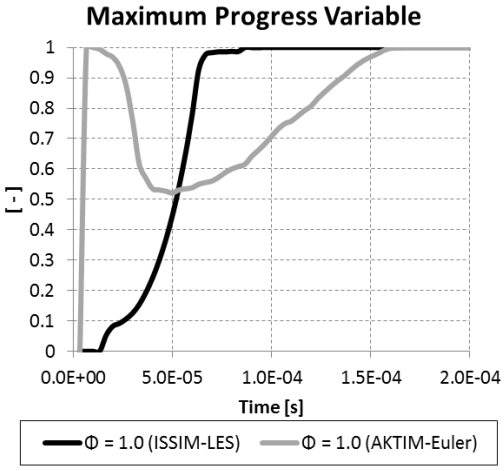

Figure 5. Maximum filtered progress variable $\tilde{c}_{max}$ for ISSIM-LES and AKTIM-Euler ignition models.

In order to gain a deeper insight into the different behavior of the two models, the maximum value of filtered progress variable $\tilde{c}_{max}$ measured in the fluid domain is reported in Figure 5. Despite the flame radius calculated with AKTIM-Euler does not significantly differ from the ISSIM-LES result, the observation of the model internal procedure shows a completely different behavior between the

two. The imposition of a fully burnt profile of burnt gases at ignition time, i.e. $\tilde{c}_{max} = 1$, is visible at the spark discharge time.

As for the ISSIM-LES case, the maximum filtered c̃ value smoothly increases from 0 (fully unburnt condition) to 1 (fully burnt). This last feature is more physically sound as a certain time is needed before the turbulent flame kernel grows to a length scale which can be correctly filtered on the adopted grid. Since ISSIM-LES model is able to simulate this subgrid-scale phase, in principle it permits a full representation of the developing flame kernel and of its interaction with the surrounding flow field. Conversely, the simulation of these phenomena would be much more limited in the first case where an established flame kernel is numerically imposed.

Finally, the ISSIM-LES model sensitivity to the intensity of the turbulent field is tested for the stoichiometric isooctane case. The baseline intensity u'=2 m/s is halved (u'=1 m/s) and doubled (u'=4 m/s), respectively. In analogy to the analysis carried out by Wang et al. [36] on a dynamic FSD model, these test cases are intended to verify the model response to turbulent environment variations. In this case the α-function behavior is the object of the observation. This is reported in Figure 6 for the three analyzed cases. As expected, the increase in turbulence intensity leads to a faster flame propagation. The transition from subgrid to resolved scales is anticipated for increasing turbulence intensity levels. In particular, it is worthwhile to notice the relevantly slower α-function grow rate for the u'=1m/s case.

Flame evolution is reported in Figures 7-9 for the three cases. The resolved flame front, here expressed by the $\tilde{c} \cdot (1 - \tilde{c})$ scalar field, illustrates the progressively higher flame wrinkling and the faster propagation speed for increasing turbulence levels.

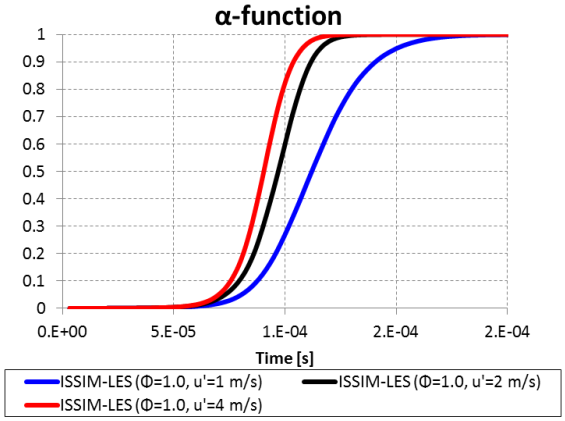

Figure 6. α-function during ignition for three turbulence intensities.

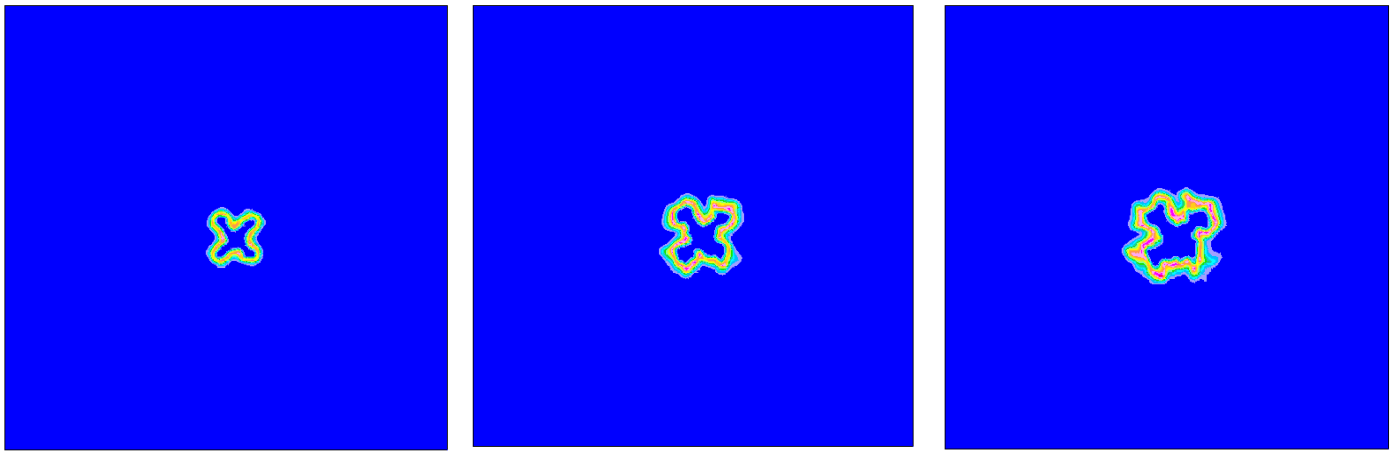

Figure 7. Resolved flame front $\tilde{c} \cdot (1 - \tilde{c})$ for ISSIM-LES ignition model at 0.33 ms after ignition time. Initial turbulence intensity: u'=1 m/2 (left), u'=2 m/s (middle) and u'=4 m/s (right).

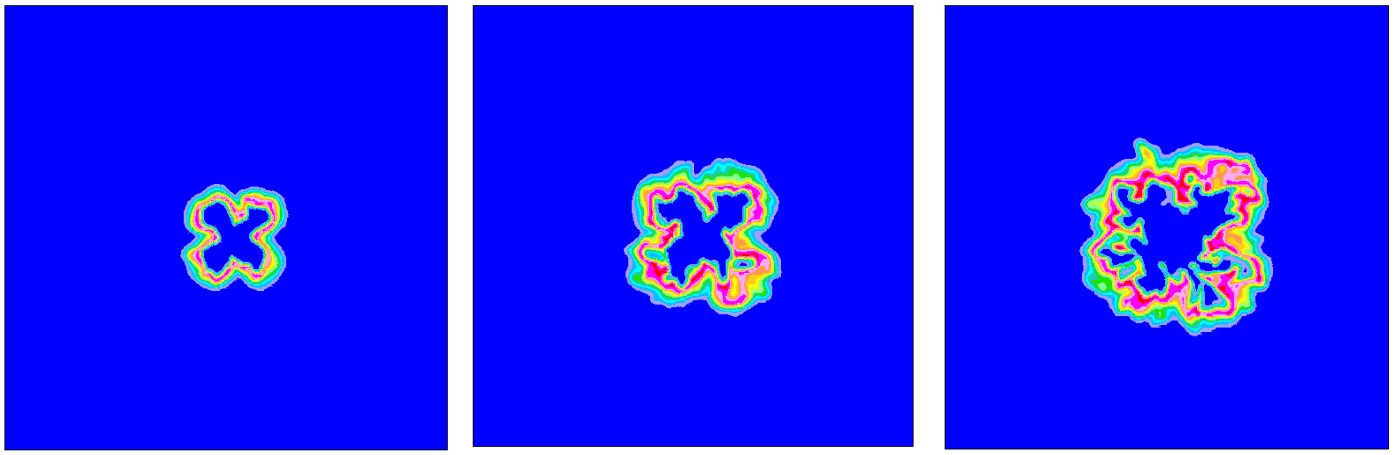

Figure 8. Resolved flame front $\tilde{c} \cdot (1 - \tilde{c})$ for ISSIM-LES ignition model at 0.66 ms after ignition time. Initial turbulence intensity: u'=1 m/2 (left), u'=2 m/s (middle) and u'=4 m/s (right).

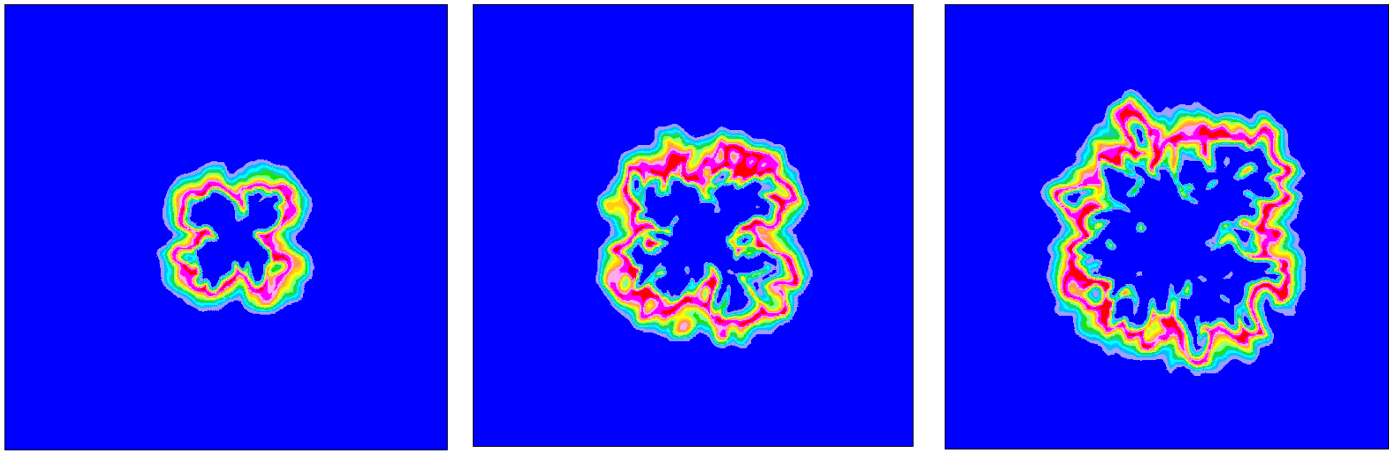

Figure 9. Resolved flame front $\tilde{c} \cdot (1 - \tilde{c})$ for ISSIM-LES ignition model at 1 ms after ignition time. Initial turbulence intensity: u'=1 m/2 (left), u'=2 m/s (middle) and u'=4 m/s (right).

Engine Cases

The analyzed unit is a V8 SI engine which is currently under production. Fuel is directly injected in the cylinder through a wall-guided strategy, thanks to a multi-hole fuel injector mounted between the intake valves. The cylinder head has 4 valves per cylinder and the bore-to-stroke ratio is slightly larger than 1. A wide campaign of experimental acquisition is carried out at the 7000 rpm W.O.T. peak power condition, which is indicated as Knock-Limited Spark Advance (KLSA) by pressure measurements carried out for each cylinder by means of flush-mounted pressure transducers. Further engine details are confidential data of the engine manufacturer.

A set of ten consecutive full cycles is calculated with ISSIM-LES ignition model. The initial condition for the simulation is a converged RANS result of the same operating point, and a first LES full cycle is discarded in order to consider a LES dataset which is independent of the change in the turbulent kinetic energy definition when switching from RANS to LES approach. The calculated cycles are obtained with the same SA as the experiments and they are compared with the full dataset of 240 experimental cycles from the engine test bed.

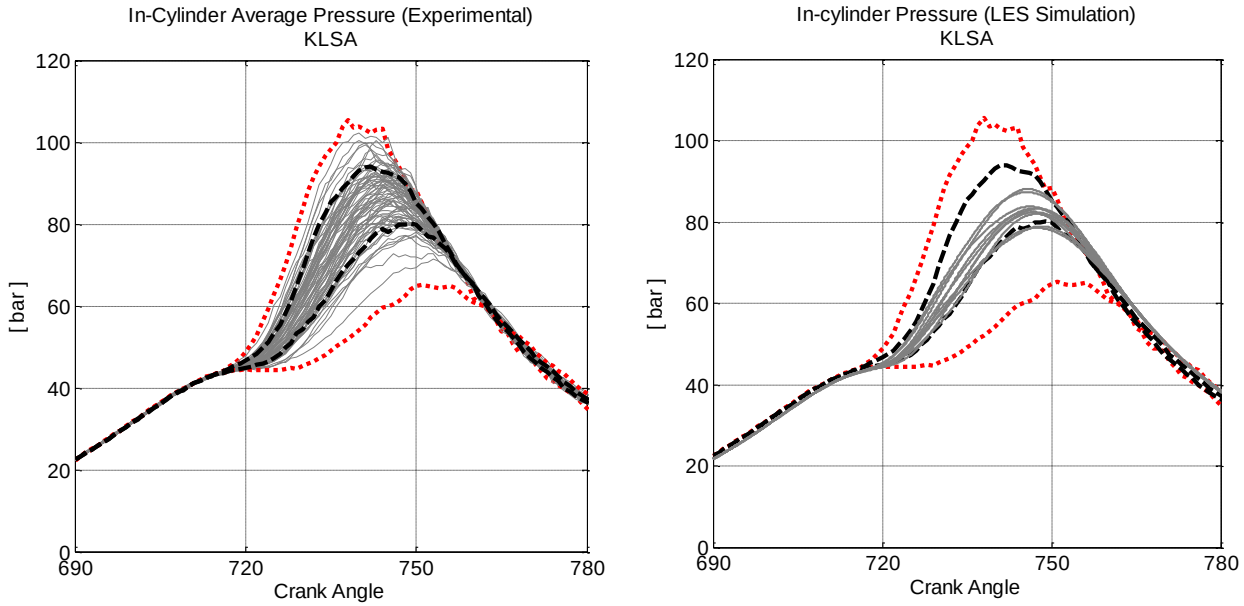

Figure 10. In-cylinder pressure traces for the analyzed condition: (left) experimental dataset of 240 consecutive cycles; (right) numeric LES dataset of 10 consecutive cycles with ISSIM-LES model. Extreme experimental cycles and $\pm\sigma$ bandwidth about the ensemble average are migrated from the experiments to allow a direct comparison.

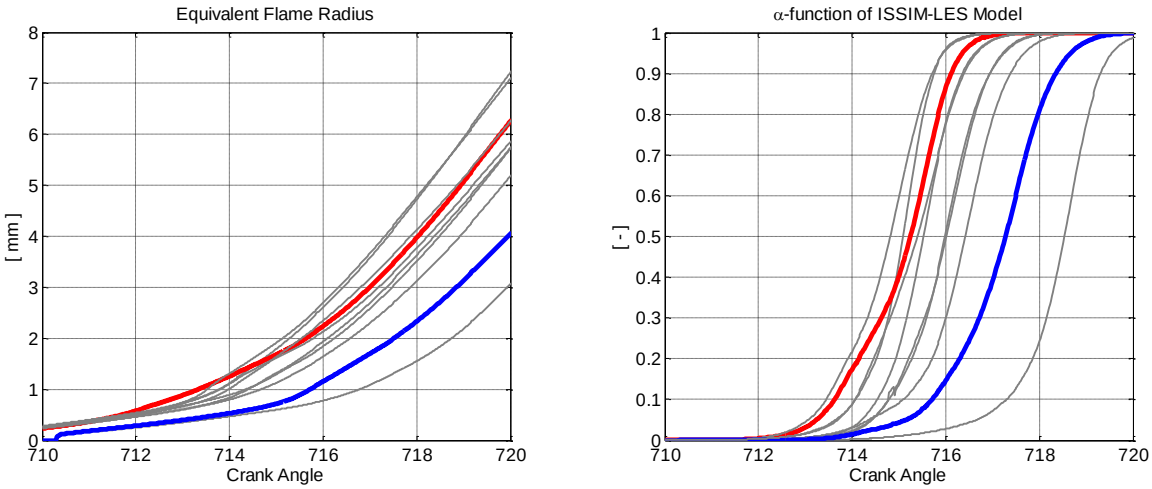

Figure 11. Flame kernel growth analysis for the 10 LES cycles with ISSIM-LES: (left) equivalent flame radius; (right) α-function evolution. Maximum peak pressure cycle (Cycle no.4, red line) and lowest one (Cycle no.10, blue line) are highlighted.

The in-cylinder pressure traces for LES simulations and experiments are reported in Figure 10. As visible, a relatively large cyclic variability of combustion is experimentally measured. The highest and lowest peak pressure cycles from the complete experimental dataset (red dashed lines) are highlighted in Figure 10 (left). Given the strong bias in the statistical sample, which is common when comparing experiments with single flow realizations by LES, a band of maximum pressure probability is identified and it is reported in Figure 10 by black dashed lines. In this study, it is arbitrarily delimited by two virtual cycles whose pressure history differs by $\pm\sigma$ from the ensemble average pressure trace. These experimental traces are also reported in Figure 10 (right) for the sake of a direct comparison between simulations and experiments.

The calculated highest peak pressure cycle, i.e. Cycle no. 4 (p_{max}=88.1 bar), and the lowest one, i.e. Cycle no. 10 (p_{max}=78.5 bar), are considered as representative of the simulated CCV and they will be recalled in the following post-process in order to better understand the origin of such different combustion behavior and the importance of the simulation of the early flame development. The output from the ISSIM-LES ignition model allows to draw a deeper analysis on the ignition phase for of the calculated cycles.

In Figure 11 (left) the equivalent flame radius (Eq. 2) is reported for the initial stages of combustion development. Even if the flame is skewed and convected since the very early stages of its appearance in the cylinder environment, due to the interaction with intense and oriented large-scale flow structures (e.g. residual tumble and squish motions), the same spherical flame shape assumption of the combustion bomb cases is used just to trace the flame size and to calculate a "flame length scale". This is used by the ISSIM-LES ignition model, in which the α-function governs the subgrid to resolved transition as described in Eq. 4. The cycle-specific α-function growth is illustrated in Figure 11 (right).

It is interesting to observe in Figure 11 (left) that none of the mentioned extreme cycles is the one measuring the fastest or slowest flame radius increase, although they lie on opposite sides of the calculated range. This is because ignition is one of the main factors contributing to the overall burn rate, although it is not the only one. The same is valid for the subgrid-to-resolved transition reported in Figure 11 (right). The comparison of the ten calculated LES cycles with the combustion indicators from the engine test bench is reported in Table 1. The calculated values are expressed in CA after Start of Combustion (CA aSOC). Data from both experiments and simulations are identically processed in order to obtain the first and second statistical moments. These are the ensemble average value and the standard deviation. Finally, the Coefficient of Variation (CoV) is used to give a more general representation of the variable fluctuation. This is calculated for a generic ϕ variable as the ratio between its standard deviation σ_ϕ and the ensemble average value $\langle\phi\rangle$ (Eq. 8).

$$CoV_\phi = \frac{\sigma_\phi}{\langle\phi\rangle} \cdot 100 \quad (8)$$

Table 1. Combustion indicators and their variability between experiments (240 cycles) and LES simulation with ISSIM-LES ignition model (10 cycles) at KLSA.

		Experiments	ISSIM-LES
MFB10	Average [CA aSOC]	20.63	20.08
	CoV	9.20%	4.75%
MFB50	Average [CA aSOC]	32.96	33.15
	CoV	7.48%	3.30%

The average values of combustion indicators for LES simulations are consistent with the experimentally measured ones, both for the initial portion of combustion (MFB10) and for the mid combustion phasing (MFB50). As for CCV, the calculated CoV values are notably lower than the corresponding experimental ones: this is attributed to the reduced size of the available dataset, which is still limited to consider adequately converged statistics. For this reason the LES database is still under development. However, since the in-cylinder pressure traces for all the calculated cycles lie within the band of maximum pressure probability (see Figure 10 (right)), the presented numerical framework is considered as able to simulate the most probable amplitude of combustion variability. The aim of this comparison with the experiments is to verify that even considering the reduced sample size the agreement with the experiments is already satisfactory, both in terms of ensemble average and standard deviation, and it can be

used to compare the response of a different ignition model. This will be the object of the next section.

Comparison Between ISSIM-LES and AKTIM-Euler Ignition Model

The ignition behavior calculated with ISSIM-LES model is compared with that obtained with a relatively simpler flame deposition model, in order to highlight the simulation improvement of the first. The chosen model for this analysis is AKTIM-Euler, whose fundamentals are recalled in the Numerical Setup section. The same ten combustion simulations, whose results with ISSIM-LES model are presented in the previous Section, are here repeated with the adoption of the AKTIM-Euler model. This comparison is intended to evaluate the response of the numerical code under the same set of cycle-dependent flow realizations and fuel stratifications. From a general perspective, the same cyclic variability of initial conditions is applied to the two models for spark-ignition and the resulting degree of combustion CCV is the object of the observation. Any disagreement between the combustion variability of two set of results is only given by the different ignition treatment. Cycle-specific peak pressure values are reported in Figure 12 and their phasing in the cycle is in Figure 13. The adoption of AKTIM-Euler ignition model leads to recurrently higher pressure peaks (Figure 12), compared to the same cold-flow simulation with flame development modelled by ISSIM-LES model. Not surprisingly, an opposite trend is found for the phasing of the maximum in-cylinder pressure in the cycles (Figure 13), which for the AKTIM-Euler model is verified earlier in the cycle than the relative ISSIM-LES value for the same spark timing. This depicts a generally faster combustion progress for the flame deposition model with respect to the ISSIM-LES one where kernel development is simulated since the beginning. This is further highlighted by the comparison reported in Table 2, where observations between the two models are carried out in terms of burnt fraction at fixed CA position which is chosen as +5 CA aTDC.

A clear trend is confirmed from the data in Table 2, and it consists in an initially faster burnt rate for the cases with AKTIM-Euler model for both the observed CA. The advance in combustion progress is such that more than twice the mass of fuel is burnt at the same CA for the AKTIM-Euler model. The reason of this excessive burn rate is to be found in the hypothesis on which the flame deposition model is based, i.e. the imposition of a finite-scale flame volume of completely burnt gases. In addition, Table 2 also gives a comparison of the cyclic variability predicted by the two ignition models. Results from ISSIM-LES ignition model exhibit a higher variability in terms of combustion progress over the 10 calculated cycles. Again, this is coherent with the physical completeness of the flame simulation since the early phase, and of its cycle-specific deviations from the ensemble average behavior. The flame development and its interaction with the local flow field are examined in detail for the two very different cycles. The same cycle (i.e. realization) is considered for the two ignition models, in order to draw coherent comparisons regarding flame development based on the same underlying flow field and fuel distribution. To this aim, Cycle no.4 is considered as representative of a “fast cycle”, since it is a realization whose peak pressure is very high/maximal both in the ISSIM-LES and in the AKTIM-Euler dataset. For the same reasons, Cycle no.10 is assumed as representative of a “slow cycle”.

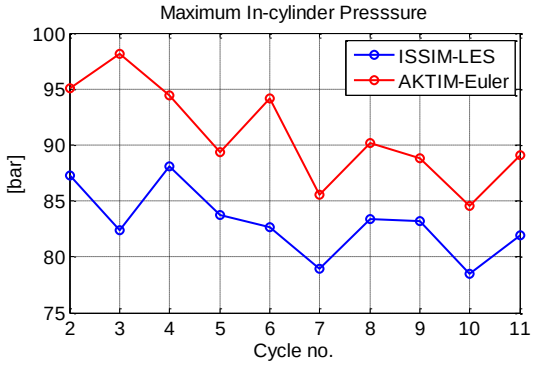

Figure 12. Cycle-specific peak pressure values for ISSIM-LES and AKTIM-Euler ignition models.

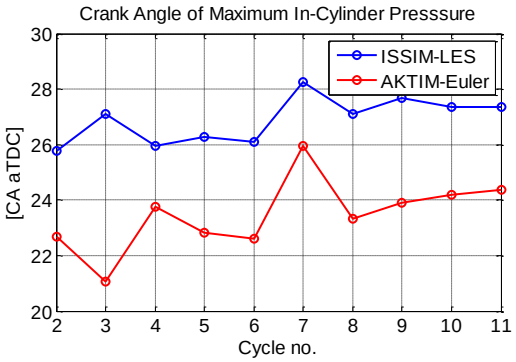

Figure 13. Cycle-specific phasing of the peak pressure angle for ISSIM-LES and AKTIM-Euler ignition models.

Table 2. Combustion progress and its variability between ISSIM-LES and AKTIM-Euler ignition model at KLSA.

		ISSIM-LES	AKTIM-Euler
+5 CA aTDC	MFB	4.94%	11.45%
	CoV	26.90%	20.93%

The equivalence ratio field on a transverse section is reported in Figure 14 for Cycle no.4 and Cycle no.10, respectively. The overall mixture enrichment guarantees a safety margin with respect to local conditions at ignition, where despite the cycle variability of fuel distribution a rich fuel-air mixture is present in the spark plug region. In Figure 15 the flame front development as simulated by ISSIM-LES model and the flame interaction with the local flow field is reported for the two cycles. The same is illustrated in Figure 16 with the adoption of AKTIM-Euler model. The relevant cyclic variability of the resolved flow field is well discernable in the analysis of the flow structures for a “fast” and a “slow” cycle. As for the former (i.e. Cycle no.4), the filtered flow field induces a balanced flame propagation on both sides of the spark plug geometry. A different situation is verified for Cycle no.10, where an intense side-oriented flow structure is responsible for flame convection towards one side of the combustion chamber (upper side in Figures 15 and 16). In this case the flame develops on one side only of the spark-plug J-electrode. In both cases, the use of the modified FSD equation of ISSIM-LES model allows the flame to be properly simulated and to interact with the details of the local flow field.

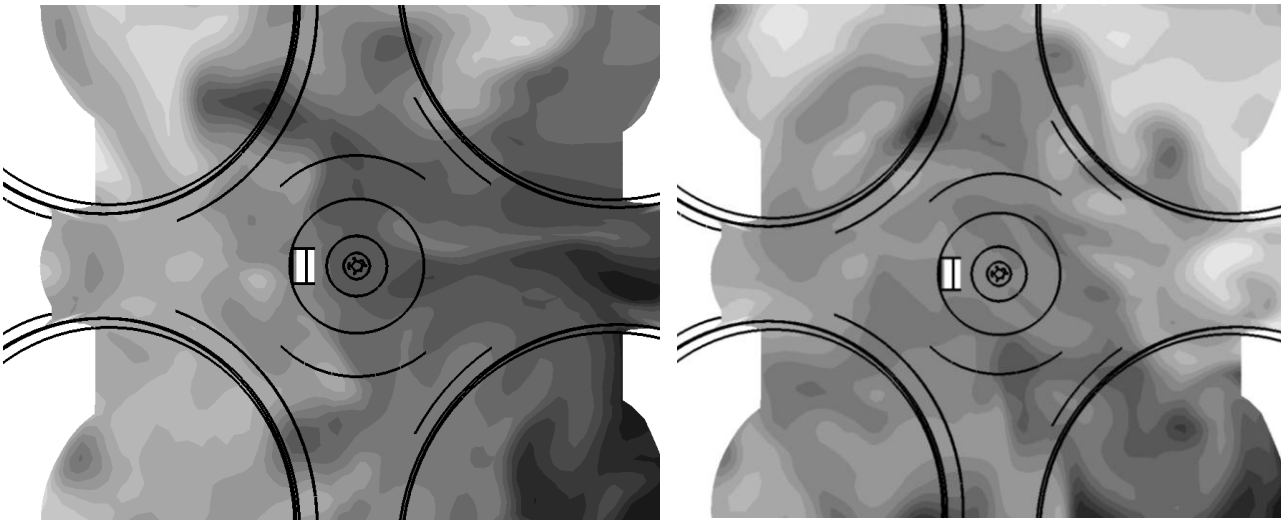

Figure 14.Equivalence ratio distribution on a transverse section containing the ignition point at -5 CA aTDC; (a) left: "fast" Cycle no.4; (b), right: "slow" Cycle no.10. Equivalence ratio scale from 0.9 (white) to 1.4 (black).

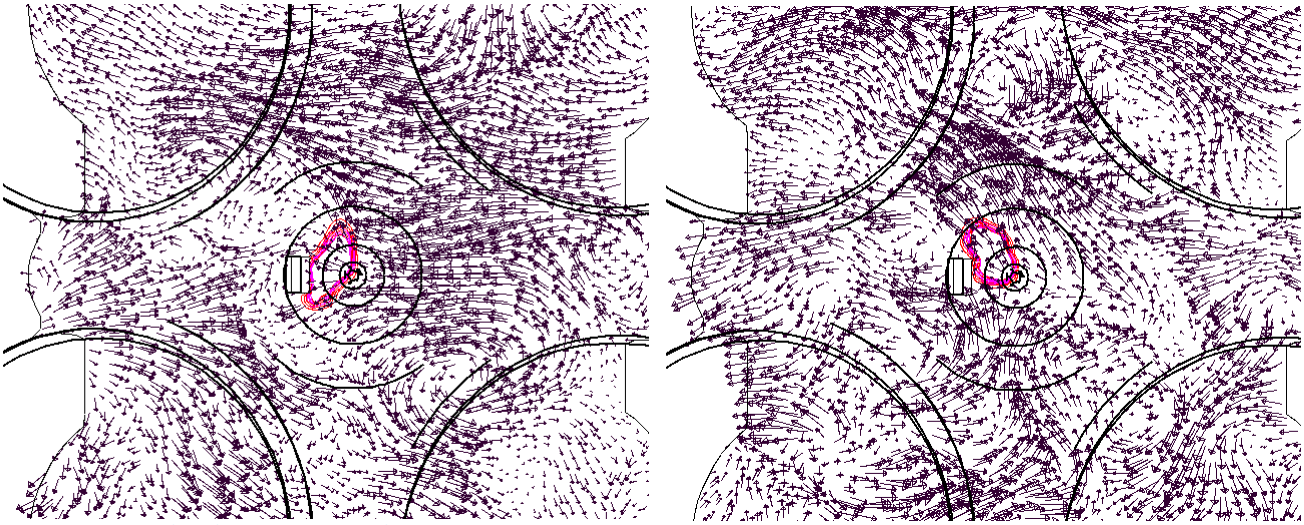

Figure 15. Filtered flow field and iso-lines of $\tilde{c}$ around 0.5 value as calculated with ISSIM-LES ignition model on a transverse section containing the ignition point at -5 CA aTDC; (a) left: "fast" Cycle no.4; (b), right: "slow" Cycle no.10.

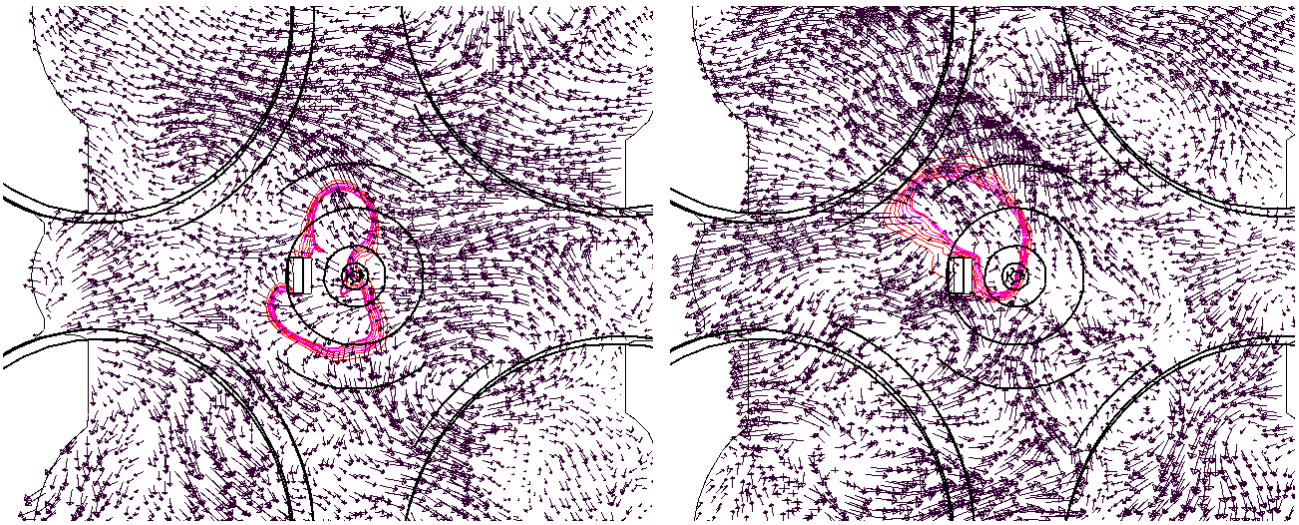

Figure 16. Filtered flow field and iso-lines of $\tilde{c}$ around 0.5 value as calculated with AKTIM-Euler ignition model on a transverse section containing the ignition point at -5 CA aTDC; (a) left: "fast" Cycle no.4; (b), right: "slow" Cycle no.10.

If the same flow and mixture realizations are provided as initial conditions for spark-ignition simulations with AKTIM-Euler model, the different behavior between the two model can be clearly seen. From a general point of view, as expected, the same trend can be observed between the combustion realizations obtained for the two chosen cycles, i.e. a balanced flame development for Cycle no.4 (Figure 16 (left)) and a side-skewed flame front for Cycle no.10 (Figure 16 (right)). This is motivated by the same flow orientation and fuel distribution as the analogous ISSIM-LES cases in Figure 14.

However, for a given realization, the comparison between the combustion simulation highlights the different ignition model behavior. In all cases, the simulation with AKTIM-Euler model presents a more developed burnt profile since ignition, i.e. a larger enflamed size. This is a direct consequence of the flame deposition nature and of the initial $\tilde{c}_{max} = 1$ hypothesis (see Figure 5). Since this is verified both for a "fast cycle" and for a "slow cycle" (Figure 15), a similar trend can be expected for all the other realizations.

A final observation is that an interesting potential result from this study is the simulation of extreme combustion events, such as poor ignition or even misfiring cycles. This is not verified in the available dataset, both due to the absence of complete misfiring events in the experimental dataset thanks to the fuel-enriched mixture and to the limited statistical size of the calculated data. The occurrence of such phenomena is usually attributed to an excessive flame stretch in the initial stages and/or to strong kernel convection by the mean flow leading to flame quenching. Therefore, their simulation is only possible with a family of ignition models such as ISSIM-LES, since the flame front evolution or quenching is handled by a dedicated transport equation considering all the cited aspects. Conversely, ignition models belonging to the flame deposition category are inherently not suited to this aim since the assumption that a flame kernel is always deposited is made.

Conclusions

A comparative study of Large-Eddy Simulation models for spark-ignition is carried out in this paper. This is motivated by the increasing interest in analyzing and limiting the cycle-to-cycle variability of turbulent combustion in modern SI units, in order to push the engine operating conditions as close as possible to the theoretical maximum efficiency limit without incurring in undesired knocking events.

To this aim the AKTIM-Euler ignition model is considered as representative of a family of ignition models based on a flame deposition at ignition time. It is compared to the more recent ISSIM-LES ignition model, which allows the simulation of the early flame kernel development thanks to the resolution of an ad-hoc modified FSD transport equation since the early stages of flame propagation.

A preliminary validation of the flame evolution given by the two models is carried out in a first test-case under homogeneous isotropic turbulence conditions. Despite the reduced difference between the two models in terms of flame expansion velocity, an opposite behavior is highlighted in terms of instantaneous imposition rather than growth simulation of an initial burnt profile.

In the second part the comparison between the two is moved to a production engine case, for which experimental acquisitions allowed to give a benchmark for the simulation of CCV in SI engines. The results with ISSIM-LES model are in excellent agreement with the experiments in terms of average combustion phasing, while the degree of CCV is still smaller, also because of the limited statistical sample from LES simulations. The calculated flow field and stratification are used as initial conditions for combustion simulations with AKTIM-Euler as well. The comparison between the two models reveals an excessive burn rate for the latter, due to the hypothesis of an instantaneous deposition of a fully burnt gas profile. Moreover, the degree of combustion CCV which is simulated in the first phase shows a relevant increase for the ISSIM-LES case, due to the simulation instead of rigid imposition of the flame kernel growth.

References

1. Fitton, J. and Nates, R., "Knock Erosion in Spark-Ignition Engines," SAE Technical Paper 962102, 1996, doi:10.4271/962102.
2. Grandin, B. and Denbratt, I., "The Effect of Knock on Heat Transfer in SI Engines," SAE Technical Paper 2002-01-0238, 2002, doi:10.4271/2002-01-0238.
3. Syrimis, M., Shigahara, K., and Assanis, D., "Correlation Between Knock Intensity and Heat Transfer Under Light and Heavy Knocking Conditions in a Spark Ignition Engine," SAE Technical Paper 960495, 1996, doi:10.4271/960495.
4. Young, M., "Cyclic Dispersion in the Homogeneous-Charge Spark-Ignition Engine—A Literature Survey," SAE Technical Paper 810020, 1981, doi:10.4271/810020.
5. Ozdor, N., Dulger, M., and Sher, E., "Cyclic Variability in Spark Ignition Engines A Literature Survey," SAE Technical Paper 940987, 1994, doi:10.4271/940987.
6. Linse, D., Kleemann, A., Hasse, C., "Probability density function approach coupled with detailed chemical kinetics for the prediction of knock in turbocharged direct injection spark ignition engines," Combustion and Flame 161 (2014) 997–1014.
7. Hasse, C., Sohm, V., Durst, B., "Numerical investigation of cyclic variations in gasoline engines using a hybrid URANS/LES modeling approach," Computers & Fluids 39 (2010) 25–48.
8. Rutland, C. J., "Large-eddy simulations for internal combustion engines- A review", International Journal of Engine Research, vol. 12, no. 5, pp. 421-451, 2011 doi: 10.1177/1468087411407248.
9. Haworth, D., "A Review of Turbulent Combustion Modeling for Multidimensional In-Cylinder CFD," SAE Technical Paper 2005-01-0993, 2005, doi:10.4271/2005-01-0993.
10. Maly, R., Vogel, M., "Initiation and Propagation of Flame Fronts in Lean CH4-Air Mixtures by the Three Modes of the Ignition Spark".
11. Fan, L., Li, G., Han, Z., and Reitz, R., "Modeling Fuel Preparation and Stratified Combustion in a Gasoline Direct Injection Engine," SAE Technical Paper 1999-01-0175, 1999, doi:10.4271/1999-01-0175.
12. Ta, Z., Reitz, R.D., "An ignition and combustion model based on the level-set method for spark ignition engine multidimensional modeling," Combustion and Flame 145 (2006) 1-15.
13. Dahms, R. N., Drake, M. C. , Fansler, T. D., Kuo T.-W., Lippert A. M., and Peters, N. ,"Modeling ignition phenomena in spray-guided spark-ignited engines," *Proc. Combust. Inst.* 32: 2743–2750 (2009), doi:10.1016/j.proci.2008.05.052.
14. Dahms, R. N., Drake, M. C., Kuo T.-W., and Peters, N., "Understanding ignition processes in spray-guided gasoline engines using high-speed laser imaging techniques & the extended spark-ignition model SparkCIMM – Part A: Spark channel processes and the turbulent flame front

propagation," *Combust. Flame* 158: 2229–2244 (2011), doi:10.1016/j.combustflame.2011.03.012.
15. Dahms, R. N., Drake, M. C., Kuo T.-W., and Peters, N., "Understanding ignition processes in spray-guided gasoline engines using high-speed imaging techniques & the extended spark-ignition model SparkCIMM – Part B: Importance of molecular fuel properties in early flame front propagation," *Combust. Flame* 158: 2245–2260 (2011), doi:10.1016/j.combustflame.2011.04.003.
16. Thobois, L., Lauvergne, R., and Poinsot, T., "Using LES to Investigate Reacting Flow Physics in Engine Design Process," SAE Technical Paper 2007-01-0166, 2007, doi:10.4271/2007-01-0166.
17. Goryntsev, D., Sadiki, A., Klein, M., Janicka, J., "Large eddy simulation based analysis of the effects of cycle-to-cycle variations on air–fuel mixing in realistic DISI IC-engines," Proceedings of the Combustion Institute 32 (2009) 2759–2766
18. Vermorel, O., Richard, S., Colin, O., Angelberger, C., Benkenida, A., Veynante, D., "Towards the understanding of cyclic variability in a spark ignited engine using multi-cycle LES," Combust. Flame 156, 8, 1525-1541 (2009).
19. Richard S., Colin O., Vermorel O., Benkenida A., Angelberger C., Veynante D. (2007) Towards large eddy simulation of combustion in spark ignition engines Proc. Combust. Inst. 31, 3059-3066.
20. Fontanesi, S., Paltrinieri, S., Tiberi, A., and D'Adamo, A., "LES Multi-cycle Analysis of a High Performance GDI Engine," SAE Technical Paper 2013-01-1080, 2013, doi:10.4271/2013-01-1080.
21. Colin, O., Truffin, K., "A spark ignition model for large eddy simulation based on an FSD transport equation (ISSIM-LES)," Proceedings of the Combustion Institute 33 (2011) 3097–3104.
22. Smagorinsky J., "General circulation experimentswith the primitive equations," Mon. Wea. Rev. 91, 99-164.
23. Angelberger, C., Poinsot, T., and Delhay, B., "Improving Near-Wall Combustion and Wall Heat Transfer Modeling in SI Engine Computations," SAE Technical Paper 972881, 1997, doi:10.4271/972881.
24. Malaguti S, Fontanesi S, Cantore G, Montanaro A and Allocca L. "Modelling of primary breakup process of a gasoline direct engine multi-hole spray," Atomization Spray 2013; 23(10): 861–888 (2013).
25. Reitz, R. and Diwakar, R., "Effect of Drop Breakup on Fuel Sprays," SAE Technical Paper 860469, 1986, doi:10.4271/860469.
26. Pope, S.B., "Ten questions concerning the large-eddy simulation of turbulent flows," New Journal of Physics 6 (2004) 35.
27. Di Mare, F., Knappstein, R., Baumann, M., "Application of LES-quality criteria to internal combustion engine flows," Computers & Fluids 89 (2014) 200–213.
28. Metghalchi, M., Keck, J.C., "Laminar burning velocity of propane-air mixtures at high temperature and pressure," Combustion and Flame 38, 143-154 (1980)
29. Fontanesi, S., Paltrinieri, S., D'Adamo, A. and Duranti, S., "Investigation of Boundary Condition and Field Distribution Effects on the Cycle-to-Cycle Variability of a Turbocharged GDI Engine Using LES," Oil & Gas Science and Technology – Rev. IFP Energies nouvelles, Vol. 69 (2014), No. 1, pp. 107-128 DOI: 10.2516/ogst/2013142.
30. Fontanesi, S., D'Adamo, A., Paltrinieri, S., Cantore, G. et al., "Assessment of the Potential of Proper Orthogonal Decomposition for the Analysis of Combustion CCV and Knock Tendency in a High Performance Engine," SAE Technical Paper 2013-24-0031, 2013, doi:10.4271/2013-24-0031.
31. Fontanesi, S., d'Adamo, A., Rutland, C.J., "Large-Eddy simulation analysis of spark configuration effect on cycle-to-cycle variability of combustion and knock," International Journal of Engine Research, April 2015; vol. 16, 3: pp. 403-418., first published on January 9, 2015.
32. Lawes, M., Ormsby, M.P., Sheppard, C.G.W. and Woolley, R. "Variation of turbulent burning rate of methane, methanol, and iso-octane air mixtures with equivalence ratio at elevated pressure," Comb. Sc. and Techn., 177 (7). pp. 1273-1289 (2005).
33. Gillespie, L., Lawes, M., Sheppard, C., and Woolley, R., "Aspects of Laminar and Turbulent Burning Velocity Relevant to SI Engines," SAE Technical Paper 2000-01-0192, 2000, doi:10.4271/2000-01-0192.
34. Bradley, D., M. Lawes, M.S. Mansour "Correlation of turbulent burning velocities of ethanol–air, measured in a fan-stirred bomb up to 1.2 MPa," Combustion and Flame 158 ,123–138, (2011).
35. Bradley, D., Gaskell, P.H. and Gu, X.J., 'Burning velocities, Markstein lengths and flame quenching for spherical methane-air flames: a computational study', Combustion and Flame, 104:176-198, 1996.
36. Wang, G., Boileau, M., Veynante, D. and Truffin, K., "Large eddy simulation of a growing turbulent premixed flame kernel using a dynamic flame surface density model, "Combustion and Flame 159 (2012) 2742–2754.

Contact Information

Alessandro d'Adamo, PhD
Department of Engineering "Enzo Ferrari", University of Modena and Reggio Emilia
Via Vivarelli 10 - 41122 Modena (Italy)
Ph. +39 059 2056115
Fax: +39 059 2056126
alessandro.dadamo@unimore.it

Acknowledgments

The authors acknowledge and thank CD-adapco for close support on the implementation and testing of the ISSIM-LES model.

Definitions/Abbreviations

AKTIM	Arc and Kernel Tracking Ignition Model
ALE	Arbitrary Lagrangian-Eulerian
aSOC	After Start of Combustion
aTDC	After Top Dead Center
CA	Crank Angle
CCV	Cycle-to-Cycle Variability
DPIK	Discrete Particle Ignition Kernel
ER	Energy Resolution
FSD	Flame Surface Density
GDI	Gasoline Direct Injection
ISSIM	Imposed Stretch Spark-Ignition Model
KLSA	Knock-Limited Spark Advance
LES	Large-Eddy Simulation
RANS	Reynolds-Averaged Navier-Stokes
SA	Spark Advance
SI	Spark-Ignition
TDC	Top Dead Center